

Enhancing non-enzymatic glucose electrochemical sensing performance with ZnO@ZIF-67 nanoarrays

Lin-an Cao^{a,*}, Min Wei^a, Zhiqiang Wu^a, Zhifeng Zhang^a, Dailian Wang^a, Tiaobin Zhao^a, Lin Hu^b

^a School of Chemistry and Chemical Engineering, NingXia Normal University, Guyuan 756000 China

^b Guyuan Maternal and Child Health Care Hospital, Guyuan 756000 China

*Corresponding author, e-mail: caolinan136@163.com

Received 2 Apr 2023, Accepted 13 Jan 2025

Available online 1 May 2025

ABSTRACT: Nanostructured metal oxide (MOX) composites exhibit significant potential for non-enzymatic glucose detection. This study introduces a novel metal oxide nanocomposite, ZnO@ZIF-67 core-shell nanoarrays, as an electrochemical enzyme-free glucose sensor electrode material, synthesized via a straightforward hydrothermal method. In this configuration, the ZIF-67 shell, characterized by its porous structure and abundant catalytically active metal centers, not only facilitates the preconcentration of glucose molecules but also offers a substantial number of catalytic active sites for glucose oxidation. Consequently, the ZnO@ZIF-67 composite demonstrates a sensitivity that is 4.5 times greater and a limit of detection that is 3 times lower for glucose compared to pristine ZnO nanoarrays. Furthermore, the ZnO@ZIF-67-based electrochemical sensor exhibits remarkable anti-interference capabilities and long-term stability. The design strategy of employing a MOX@MOF core-shell structure for electrode materials presents a novel approach for enhancing the performance of glucose monitoring.

KEYWORDS: ZnO@ZIF-67, composites, non-enzymatic electrodes, glucose electrochemical sensors

INTRODUCTION

Diabetes mellitus is a chronic condition that significantly impacts individuals' health and quality of life [1–3]. Consequently, the development of simple, rapid, and accurate methods for quantitatively detecting glucose levels in blood is of considerable importance, as it enables patients to make timely adjustments to their dietary habits. Furthermore, such methods hold substantial value for the clinical early detection and treatment of diabetes [4, 5]. Over the past few decades, numerous techniques have been employed to monitor blood glucose levels, including colorimetric methods [6], surface plasmon resonance [7], fluorescence [8], gas chromatography [9], and electrochemical sensors [10]. Among these various detection techniques, electrochemical sensing has garnered increasing attention due to its exceptional sensitivity, rapid response time, simplicity of instrumentation, capability for real-time monitoring, and portability [11, 12]. Based on the materials used for the electrodes, glucose electrochemical sensors can be categorized into enzymatic and non-enzymatic sensors. While enzyme-based glucose sensors exhibit remarkable sensitivity and selectivity towards the target analyte, their widespread application is hindered by factors such as high manufacturing costs, complex immobilization processes, and instability [13, 14]. Therefore, the development of non-enzymatic glucose sensors has generated significant research interest aimed at addressing the inherent limitations associated with enzyme-based sensors [15].

The rapid advancements in nanotechnology have

facilitated the extensive investigation of a wide array of nanomaterials, including metals [16], alloys [17], metal hydroxides [18], metal oxides [19], carbon materials, and their nanocomposites [20], in the context of glucose electrochemical sensing [21]. Notably, significant research efforts have been directed towards nanostructured metal oxides, such as zinc oxide (ZnO), which are recognized for their favorable electrocatalytic properties, cost-effectiveness, and remarkable stability [22, 23]. Furthermore, modified ZnO nanostructures incorporating metal nanoparticles [14], other metal oxides [24], and carbon materials [25] have also been investigated. Nevertheless, the majority of these modification materials remain constrained by their inherent structural characteristics, which poses challenges in enhancing charge transfer kinetics through the topology of the electrode material [26].

Metal-organic frameworks (MOFs) represent a class of porous crystalline materials that are composed of metal centers coordinated with organic ligands through coordination bonds [27–29]. These frameworks exhibit an ultra-large specific surface area, high density, and uniformly dispersed catalytic active sites, along with adjustable apertures, which render them highly attractive in the field of sensing [30]. In recent years, MOFs have been engineered into a ZnO@MOF core-shell structure, which demonstrates unique physical and chemical properties in sensing applications, attributable to the exceptional functionalities of the shell MOF [31–33]. Given these characteristics, ZnO@MOF structures may serve as promising candidates for efficient electrochemical sensor electrode components; however, they have received limited attention in the

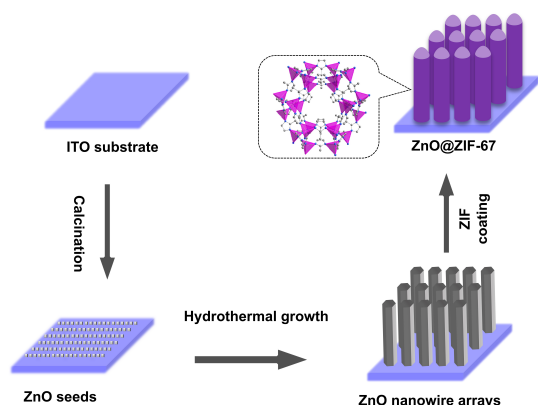


Fig. 1 Schematic representation of the preparation process for ZnO@ZIF-67 nanoarrays.

literature.

In this study, we synthesized ZnO@ZIF-67 (where ZIF-67 = $[\text{Co}(\text{MIM})_2]_n$ and MIM = 2-methylimidazole) core-shell nanoarrays on an indium tin oxide (ITO) substrate to serve as an enzyme-free electrochemical sensor electrode material. We examined its application for the detection of trace glucose. Due to the porous structure and catalytically active metal centers of shell ZIF-67 which can simultaneously preconcentrate and catalyze target molecule, the properties and stability of this electrochemical sensor were determined.

MATERIALS AND METHODS

The preparation process of ZnO@ZIF-67 was based on the methodology described by Yao et al [32], as illustrated in Fig. 1. Initially, a layer of ZnO seed was fabricated on an indium tin oxide (ITO) substrate. Subsequently, ZnO nanowire arrays were synthesized using a straightforward hydrothermal method. Finally, a thin film of ZIF-67 was deposited onto the ZnO nanowire arrays through the hydrothermal process. It is noteworthy that all ITO substrates utilized in this study are commercially available.

Materials

All chemicals utilized were of commercial grade, without any additional purification processes. ITO substrates were acquired from Henan Guluo Optoelectronics Technology Co., Ltd. (China). The following reagents were sourced from Sinopharm Chemical Reagent Co., Ltd. (China): ethanol, hexamethylenetetramine (HMT), zinc acetate dihydrate ($\text{ZnAc}_2 \cdot 2\text{H}_2\text{O}$), cobalt(II) nitrate hexahydrate ($\text{Co}(\text{NO}_3)_2 \cdot 6\text{H}_2\text{O}$), N,N-Dimethyl formamide (DMF), glucose, ascorbic acid (AA), uric acid (UA), and dopamine (DA).

Synthesis of zinc oxide nanowire arrays

The substrates employed for the cultivation of ZnO nanowire arrays were ITO with dimensions of $1 \times 1 \text{ cm}^2$. Initially, a ZnO seed layer was deposited onto the conductive side of the ITO substrate through the thermal decomposition of zinc acetate in a tube furnace at 350°C for 0.5 h. Subsequently, the seeded substrate was immersed in an aqueous solution containing 0.01 M $\text{ZnAc}_2 \cdot 2\text{H}_2\text{O}$ and 0.01 M HMT, with a total volume of 16 ml, within a Teflon-lined stainless steel autoclave. The autoclave was maintained at 95°C for 16 h. Finally, the substrate was thoroughly rinsed with deionized (DI) water and subjected to calcination in a tube furnace for 2 h at 550°C .

Synthesis of ZnO@ZIF-67 nanowire arrays

In the synthesis of ZnO@ZIF-67 nanowire arrays, ZIF-67 was deposited onto a template of ZnO nanowire arrays utilizing the hydrothermal method. Initially, 0.004 g of $\text{Co}(\text{NO}_3)_2 \cdot 6\text{H}_2\text{O}$ (0.86 mM) and 0.040 g of 2-methylimidazole (30.4 mM) were dissolved in a 16 ml mixed solution of DMF and DI water, with a volume ratio of DMF to H_2O of 13.5:2.5. Subsequently, the prepared ZnO nanowire arrays were immersed in the aforementioned mixed solution within a Teflon-lined stainless steel autoclave. The autoclave was maintained at 60°C for 2 h, after which the nanowire arrays were thoroughly washed with DI water and ethanol. Finally, the ZnO@ZIF-67 nanowire arrays were air-dried at room temperature.

Characterization

The morphology of ZnO and ZnO@ZIF-67 was examined using a field emission scanning electron microscope (FE-SEM) at an accelerating voltage of 10 kV, employing the JSM-7610F microscope manufactured by Japan Electronics Co., Ltd., Tokyo, Japan. Transmission electron microscopy (TEM) images were acquired using a FEI Talos F200S microscope (FEI Co., Oregon, USA) at an accelerating voltage of 200 kV to investigate the structural characteristics of the ZnO@MOF material. The phase and crystal structures of the materials were analyzed through X-ray diffraction (XRD) patterns, which were recorded with a Bruker AXS D8 X-ray diffractometer (Bruker, Germany) utilizing a copper target ($\text{Cu K}\alpha$ radiation: $\lambda = 1.5418 \text{ \AA}$) at room temperature. X-ray photoelectron spectroscopy (XPS) was performed using a Thermo Scientific K-Alpha spectrometer (Thermo Fisher Scientific, Massachusetts, USA), employing $\text{Al K}\alpha$ X-rays ($h\nu = 1486.6 \text{ eV}$; 12 kV, 6 mA) as the excitation source. Data analysis was conducted using the Avantage XPS software program.

Electrochemical testing

Electrochemical measurements for glucose sensing were conducted utilizing a CHI 660E electrochemical

workstation (Chenhua, China). A conventional three-electrode configuration was employed, comprising an Ag/AgCl reference electrode, a platinum mesh counter electrode ($1 \times 1 \text{ cm}^2$), and an ITO substrate with samples serving as the working electrode. The ZnO/ITO and ZnO@ZIF-67/ITO electrodes were examined as glucose sensors in an alkaline medium. Cyclic voltammetry (CV) and chronoamperometric (I-t) measurements were performed in 30 ml of 0.1 M NaOH electrolyte. All electrochemical experiments were carried out at room temperature.

Preparation of human blood serum

The human blood was placed in a water bath at 45°C for 10 min, followed by centrifugation at 5000 rpm for an additional 10 min. Human blood serum was obtained by collecting the supernatant. The resulting serum was stored at temperatures ranging from -5°C to -20°C .

RESULTS AND DISCUSSION

Field emission scanning electron microscopy (FE-SEM) is a sophisticated technique utilized for the morphological characterization of materials, enabling the acquisition of high-resolution microstructural images. Fig. 2a and 2b present FE-SEM images of ZnO and ZnO@ZIF-67 nanowire arrays, respectively. It is evident that the ZnO nanowires exhibit vertical growth on the ITO substrate, maintaining a uniform length. Similarly, the ZnO@ZIF-67 nanowires retain their original morphology; however, the surface texture becomes noticeably rougher due to the ZIF-67 coating compared to pure ZnO. A clearer observation of the nanowire arrays is provided in the cross-sectional view depicted in Fig. S1. As illustrated in Fig. 2c, TEM measurements offer detailed insights into the core-sheath structure of ZnO@ZIF-67. The ZnO core and the MOF sheath exhibit a significant contrast difference, attributable to the greater atomic mass of the ZnO core relative to that of the MOF sheath. Additionally, the thickness of the MOF sheath is approximately 10 nm. Fig. 2d displays the powder P-XRD patterns of the ZnO@ZIF-67 nanocomposite, derived from powders collected from multiple ITO substrates, as the quantity of ZnO@ZIF-67 grown on the ITO is minimal. The diffraction peaks corresponding to (011), (002), and (112) are attributed to ZIF-67, while the peaks at (100), (002), and (101) are associated with hexagonal ZnO. The P-XRD results indicate the coexistence of crystalline ZnO and ZIF-67 within the synthesized nanocomposite.

The surface chemical composition and elemental valence of the ZnO@ZIF-67 nanohybrid were analyzed using XPS. As depicted in Fig. 3a, the survey scan spectrum of ZnO@ZIF-67 reveals the presence of carbon (C), oxygen (O), nitrogen (N), cobalt (Co), and zinc (Zn) elements, thereby confirming the successful synthesis of the composite materials. The binding

energies of Co 2p, N 1s, and C 1s correspond well to the values reported for ZIF-67 [34]. The high-resolution Co 2p spectrum of ZnO@ZIF-67, shown in Fig. 3b, displays two prominent peaks at 781.12 eV and 796.92 eV, which are attributed to Co $2p_{3/2}$ and Co $2p_{1/2}$ (in the +2 oxidation state), respectively. These peaks are accompanied by two shake-up satellite peaks at 785.2 eV and 802.5 eV. Furthermore, as illustrated in Fig. 3c, the high-resolution spectrum of Zn 2p exhibits two dominant peaks at 1021.94 eV (Zn $2p_{3/2}$) and 1045.02 eV (Zn $2p_{1/2}$), indicating that the valence state of Zn is also +2 and that the zinc is derived from ZnO [35]. The N 1s spectrum of ZnO@ZIF-67, located at 399.4 eV, is symmetrical, as shown in Fig. 3d, and is attributed to the N-Co bond within the ZIF structure.

The glucose sensing performance of the ZnO@ZIF-67/ITO electrode was assessed using electrochemical methods, with ZnO/ITO and bare ITO serving as control samples. All experiments were conducted within a three-electrode system, with further details provided in the Methods section. To evaluate the electrochemical properties and sensing capabilities of the electrodes in glucose oxidation, Fig. 4a presents the cyclic voltammetry (CV) curves for the ITO, ZnO/ITO, and ZnO@ZIF-67/ITO electrodes in a 0.1 M NaOH solution containing 2 mM glucose, recorded at a scan rate of 50 mV/s over a potential range of 0.2 to 0.8 V. It is evident that the ITO electrode exhibited a low current density in the absence of glucose, with only a minor change in current upon the addition of glucose. The current signal and sensitivity to glucose for the ZnO/ITO electrode showed a slight increase, suggesting that the ZnO nanowire arrays facilitate electron transfer during the glucose oxidation process to a certain extent. Notably, the CV curves for the ZnO@ZIF-67/ITO electrode displayed significant alterations compared to the control samples. The current signal markedly increased, particularly in the higher potential range, and the current response to glucose was also greater than that observed for the ITO and ZnO/ITO electrodes individually. These results indicate that ZIF-67 contributes a porous structure and a large specific surface area, enhancing the material's adsorption capacity. The adsorption of the MOF allows for a greater number of glucose molecules to participate in the redox reaction, thereby improving response sensitivity. Additionally, the cobalt metal center within ZIF-67 exhibits catalytic properties, as reported by Yao et al [32], which further facilitates efficient electron transfer and synergistically enhances the current signal response.

To assess the performance of the prepared sensors for glucose detection, chronoamperometric (I-t) analysis was employed to evaluate key parameters such as sensitivity, linear detection range, and selectivity. As illustrated in the CV curves presented in Fig. 4a, a significant change in current density was observed

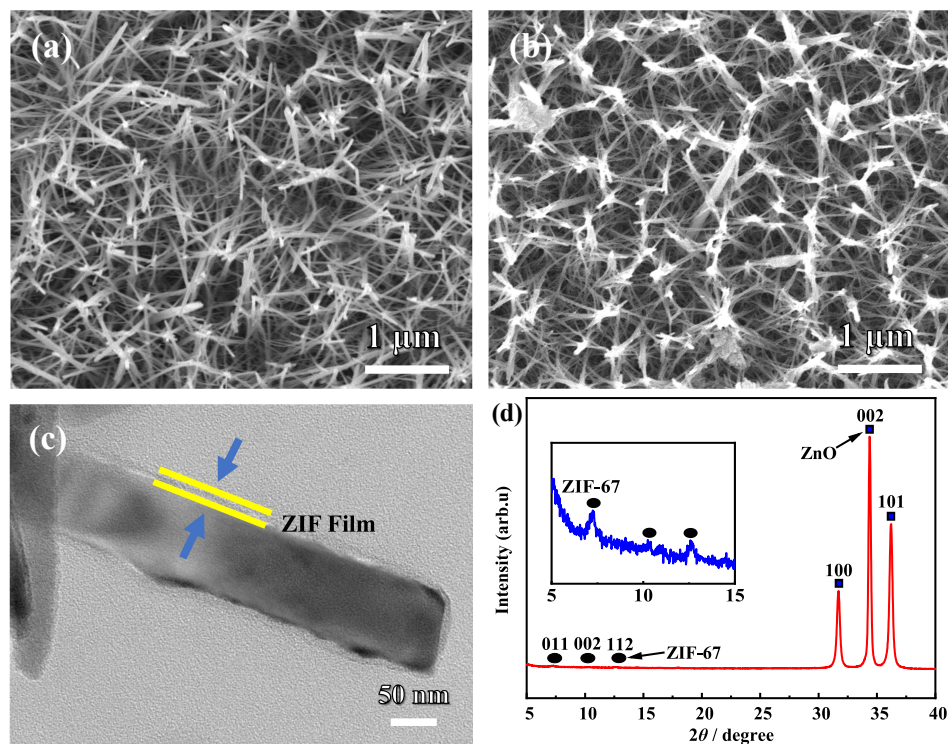


Fig. 2 FE-SEM images of (a) ZnO and (b) ZnO@ZIF-67 nanowire arrays. (c) TEM image of ZnO@ZIF-67 nanowires. (d) P-XRD patterns of ZnO@ZIF-67 nanowire arrays collected from ITO substrates (the inset shows the magnified image from 5–15 degree).

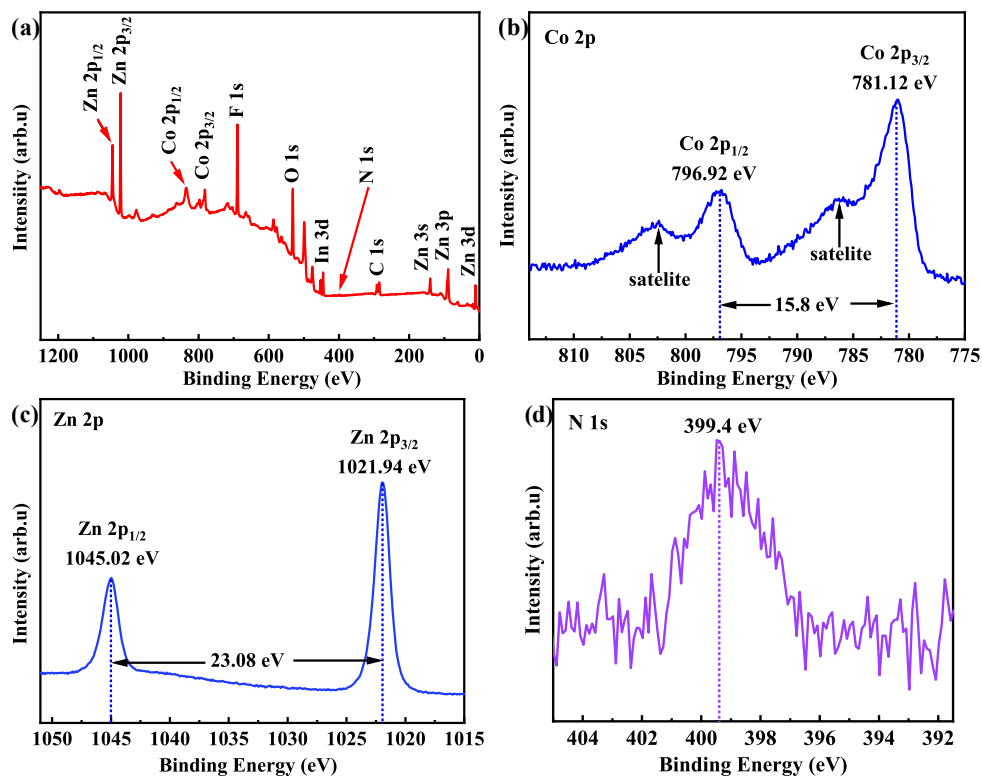


Fig. 3 (a) Survey scan XPS spectra of ZnO@ZIF-67. High resolution XPS spectra of (b) Co 2p, (c) Zn 2p, and (d) N 1s.

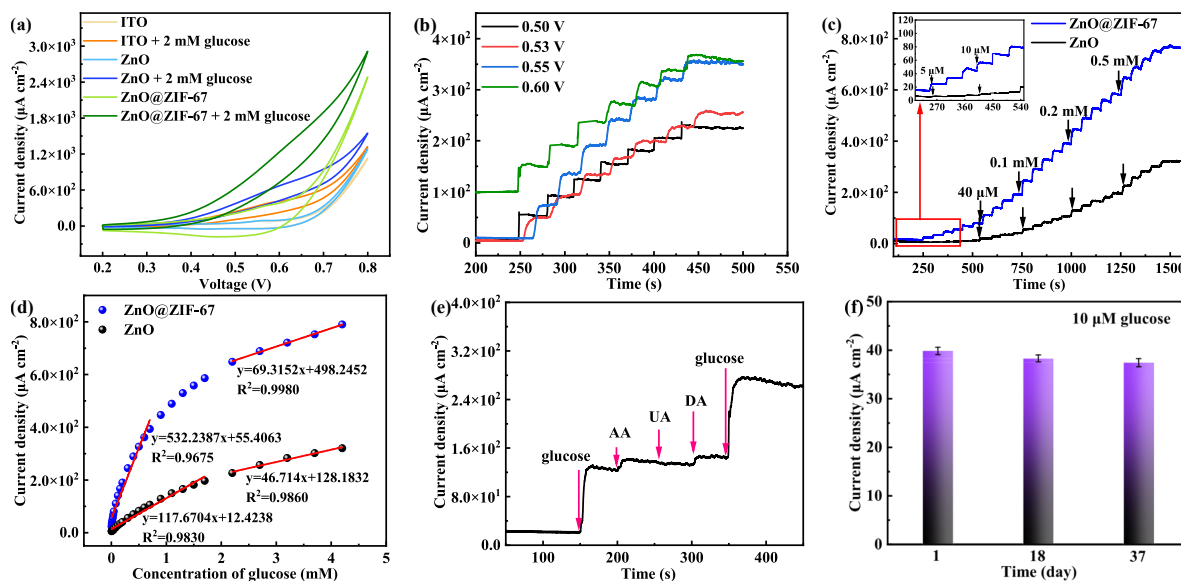


Fig. 4 (a) Cyclic voltammograms of ITO, ZnO/ITO and ZnO@ZIF-67/ITO electrodes. (b) The current response of ZnO@ZIF-67 at different potentials. (c) Amperometric curves of ZnO and ZnO@ZIF-67 to successive addition of glucose at an applied potential of 0.55 V. Inset: The time is from 200 s to 550 s. (d) The calibration curves of ZnO and ZnO@ZIF-67 sensors response to glucose. (e) Amperometric response of ZnO@ZIF-67 to successive additions of 100 μM glucose and 20 μM other interfering species at an applied potential of 0.55 V. (f) Response current of ZnO@ZIF-67 at the 1st, 18th, and 37th days, respectively.

within the potential range of 0.5 V to 0.6 V. Consequently, the ZnO@ZIF-67/ITO electrode was tested at a series of potentials, specifically 0.5 V, 0.53 V, 0.55 V, and 0.6 V, to determine the optimal potential by incrementally adding glucose. As shown in Fig. 4b, the current response to glucose was most pronounced at a working potential of 0.55 V. Therefore, 0.55 V was designated as the optimal working potential for subsequent chronoamperometric analyses in this research.

Under optimal conditions, the typical current-time (I-t) diagram for ZnO/ITO and ZnO@ZIF-67/ITO in the presence of 0.1 M NaOH, with successive additions of varying concentrations of glucose, is presented in Fig. 4c. The inset diagram illustrates an amplified portion of the I-t curves corresponding to low glucose concentrations (5 μM –45 μM). A transient and stepwise amperometric response is observed for both samples following each glucose addition within a 5-s interval. However, ZnO@ZIF-67/ITO demonstrates a significantly higher response compared to ZnO/ITO. The linear calibration relationship between current response and glucose concentration is depicted in Fig. 4d. For the ZnO/ITO electrode, two linear relationships are established within the ranges of 5 μM to 1.7 mM, exhibiting a correlation coefficient (R^2) of 0.983, and from 2.1 mM to 4.2 mM, with an R^2 of 0.986, respectively. The sensitivity, calculated from the slope of the linear calibration curve, is 117.670 $\mu\text{A mM}^{-1}\text{cm}^{-2}$ in the low concentration range and 46.714 $\mu\text{A mM}^{-1}\text{cm}^{-2}$ in the high concentration

range. As glucose concentration increases, the electrode surface becomes partially covered by adsorbed reaction intermediates, which limits the availability of active sites for incoming glucose molecules [36, 37]. Consequently, the amperometric response gradually approaches saturation, resulting in two distinct linear responses across the tested concentration range. Furthermore, the limit of detection (LOD) is estimated to be 4.8 μM , calculated using the formula: $\text{LOD} = 3 \text{SD}/S$ (where SD represents the standard deviation of the blank signal, and S denotes sensitivity). In contrast, the ZnO@ZIF-67/ITO electrode exhibits a higher sensitivity of 532.239 $\mu\text{A mM}^{-1}\text{cm}^{-2}$ in the low concentration range and a lower LOD of 1.6 μM , outperforming ZnO/ITO. This enhanced detection performance of ZnO@ZIF-67/ITO can be attributed to its ultra-large specific surface area, high density, and uniformly dispersed catalytic active sites, which facilitate glucose preconcentration and provide abundant active sites for the oxidation of glucose molecules. Although the pore size of ZIF-67 is smaller than that of the glucose molecule, glucose can still traverse the ZIF apertures due to the mobility of the 2-MIM linker [38, 39]. Additionally, the analytical performance of the ZnO@ZIF-67/ITO sensor for glucose detection is comparable to, or even superior to, other reported glucose sensors, as summarized in Table S1.

In addition to glucose, human blood contains various electroactive interfering species, including ascorbic acid (AA), uric acid (UA), and dopamine (DA), which

may compromise the accuracy of test results. However, the concentrations of these substances in the blood are typically 30 to 50 times lower than that of glucose [40]. Consequently, we assessed the anti-interference capability of ZnO@ZIF-67/ITO by analyzing the chronoamperometric response to different analytes at a potential of 0.55 V. As illustrated in Fig. 4e, a significant current response was observed upon the addition of 100 μM glucose. In contrast, the subsequent introduction of 20 μM AA, 20 μM UA, and 20 μM DA resulted in only minimal changes in current compared to that induced by glucose. This finding indicates that the proposed sensor exhibits a favorable selectivity for glucose.

Long-term stability and reproducibility are critical evaluation parameters for electrochemical sensors. To evaluate the long-term stability of the ZnO@ZIF-67/ITO sensor for glucose detection, the amperometric response of the sensor to 10 μM glucose was recorded over a period of 37 days. During this time, the electrode was stored in ambient air at room temperature. As illustrated in Fig. 4f, the sensor retained 94.9% of its original response current after 37 days of storage, demonstrating the exceptional stability of the ZnO@ZIF-67/ITO electrode. Reproducibility was assessed by measuring the current response to glucose from five identically prepared electrodes under the same conditions (see Fig. S2). The relative standard deviation (RSD) for these five electrodes was determined to be 4.98%, confirming the reproducibility of the fabricated electrochemical sensor. Additionally, repeatability was evaluated by successively measuring the current response to 10 μM glucose five times using a single electrode, resulting in an RSD of 3.86% (refer to Fig. S3). This indicates that the electrochemical sensor exhibits good repeatability.

In order to illustrate the practical application of the ZnO@ZIF-67 electrode, we employed it to detect glucose in human serum. A serum solution with a glucose concentration of 6.2 mM was prepared in advance for the experiment. Amperometric measurements were conducted three times, and the results demonstrated a significant current response to the serum, as depicted in Fig. S4. The glucose concentration in the serum was calculated and is presented in Table S2. The recovery rates ranged from 98.71% to 105.48%, indicating that our sensor exhibits considerable promise for practical sample testing, characterized by exceptional reliability.

CONCLUSION

In summary, we have successfully developed an enzyme-free electrochemical glucose sensor utilizing ZnO@ZIF-67/ITO for the first time. The incorporation of a MOF thin film has significantly altered the surface structure and electrochemical sensing performance of ZnO in relation to glucose. Specifically, the following enhancements were observed: (1) the porous MOF, characterized by a large specific surface

area, increased the electrode's adsorption capacity for glucose molecules; (2) the sensitivity of ZnO@ZIF-67 was improved 4.5 times compared to pure ZnO; and (3) the limit of detection was reduced 3 times. Furthermore, the MOX@MOF electrode material demonstrated excellent stability. This study confirms that the integration of multifunctional MOF materials with electroactive metal oxides represents a promising strategy for the development of high-performance non-enzymatic electrochemical glucose sensors, with potential applications in the analysis of real samples.

Appendix A. Supplementary data

Supplementary data associated with this article can be found at <https://dx.doi.org/10.2306/scienceasia1513-1874.2025.033>.

Acknowledgements: This work was supported by the National Natural Science Foundation of China (No: 51402293), Ningxia Autonomous Region Key R&D Program (Special for Talent Introduction) (No: 2021BEB04026, 2021BEB04003), Natural Science Foundation of Ning Xia (No: 2022AAC03303), The Key R&D Program of Ningxia Hui Autonomous Region (No: 2022BDE03013), and Ningxia Normal University Engineering Center Project (No: HGZD22-19, HGZD22-25, HGZD22-27).

REFERENCES

1. Fralick M, Jenkins AJ, Khunti K, Mbanya JC, Mohan V, Schmidt MI (2020) Global accessibility of therapeutics for diabetes mellitus. *Nat Rev Endocrinol* **18**, 199–204.
2. Hussain MH, Fook LP, Sanira Putri MK, Tan HL, Abu Bakar NF, Radacsi N (2021) Advances on ultra-sensitive electrospun nanostructured electrochemical and colorimetric sensors for diabetes mellitus detection. *Nano Mater Sci* **3**, 321–343.
3. Ye Z, Miao F, Tao B, Zang Y, Chu PK (2021) Facile synthesis of ZnO doped with Au nanoparticles for sensitive and reliable photoelectrochemical detection of glucose. *Ionics* **27**, 4449–4459.
4. Zhang J, Chen L, Yang K (2019) *In situ* synthesis of CuO nanoparticles decorated hierarchical Ce-metal-organic framework nanocomposite for an ultrasensitive non-enzymatic glucose sensor. *Ionics* **25**, 4447–4457.
5. Reghunath R, Devi K, Singh KK (2021) Recent advances in graphene based electrochemical glucose sensor. *Nano-Struct Nano-Objects* **26**, 100750.
6. Hui G, Ying Y (2017) Quantitative rapid analysis method for ofloxacin in raw milk based on molecule-specific recognition and electrochemical impedance spectrum. *T ASABE* **60**, 1439–1443.
7. Lyandres O, Yuen JM, Shah NC, VanDuyne PR, Walsh JT, Glucksberg MR (2008) Progress toward an *in vivo* surface-enhanced Raman spectroscopy glucose sensor. *Diabetes Technol Ther* **10**, 257–265.
8. Larsen T (2015) Fluorometric determination of free glucose and glucose 6-phosphate in cows' milk and other opaque matrices. *Food Chem* **166**, 283–286.
9. Xie WQ, Gong YX, Yu KX (2017) Rapid quantitative detection of glucose content in glucose injection by reaction headspace gas chromatography. *J Chromatogr A* **1520**, 143–146.

10. Charoenkitamorn K, Yakoh A, Jampasa S, Chaiyo S, Chailapakul O (2020) Electrochemical and optical biosensors for biological sensing applications. *ScienceAsia* **46**, 245–253.
11. Anu Prathap MU, Kaur B, Srivastava R (2019) Electrochemical sensor platforms based on nanostructured metal oxides, and zeolite-based materials. *Chem Rec* **19**, 883–907.
12. Ko M, Mendecki L, Eagleton AM, Durbin CG, Stolz RM, Meng Z, Stolz KM (2020) Employing conductive metal-organic frameworks for voltammetric detection of neurochemicals. *J Am Chem Soc* **142**, 11717–11733.
13. Lee H, Hong YJ, Baik S, Hyeon T, Kim DH (2018) Enzyme-based glucose sensor: From invasive to wearable device. *Adv Healthc Mater* **7**, e1701150.
14. Miao F, Wu W, Miao R, Cong W, Zang Y, Tao B (2018) Graphene/nano-ZnO hybrid materials modify Ni-foam for high-performance electrochemical glucose sensors. *Ionics* **24**, 4005–4014.
15. He G, Wang L (2018) One-step preparation of ultra-thin copper oxide nanowire arrays/copper wire electrode for non-enzymatic glucose sensor. *Ionics* **24**, 3167–3175.
16. Tee SY, Teng CP, Ye E (2017) Metal nanostructures for non-enzymatic glucose sensing. *Mater Sci Eng C Mater Biol Appl* **70**, 1018–1031.
17. Yang H, Wang Z, Li C, Xu C (2017) Nanoporous PdCu alloy as an excellent electrochemical sensor for H₂O₂ and glucose detection. *J Colloid Interface Sci* **491**, 321–328.
18. Li H, Zhang L, Mao Y, Wen C, Zhao P (2019) A simple electrochemical route to access amorphous Co-Ni hydroxide for non-enzymatic glucose sensing. *Nanoscale Res Lett* **14**, 135.
19. Zhu H, Li L, Zhou W, Shao Z, Chen X (2016) Advances in non-enzymatic glucose sensors based on metal oxides. *J Mater Chem B* **4**, 7333–7349.
20. Wang F, Chen X, Chen L, Yang J, Wang Q (2019) High-performance non-enzymatic glucose sensor by hierarchical flower-like nickel(II)-based MOF/carbon nanotubes composite. *Mater Sci Eng C Mater Biol Appl* **96**, 41–50.
21. Sehat E, Altintas Z (2020) Significance of nanomaterials in electrochemical glucose sensors: An updated review (2016–2020). *Biosens Bioelectron* **159**, 112165.
22. George JM, Antony A, Mathew B (2018) Metal oxide nanoparticles in electrochemical sensing and biosensing: A review. *Mikrochim Acta* **185**, 358.
23. Beitollahi H, Tajik S, Garkani Nejad F, Safaei M (2020) Recent advances in ZnO nanostructure-based electrochemical sensors and biosensors. *J Mater Chem B* **8**, 5826–5844.
24. Haghparas Z, Kordrostami Z, Sorouri M, Rajabzadeh M, Khalifeh R (2021) Highly sensitive non-enzymatic electrochemical glucose sensor based on dumbbell-shaped double-shelled hollow nanoporous CuO/ZnO microstructures. *Sci Rep* **11**, 344.
25. Chung RJ, Wang AN, Liao QL, Chuang KY (2017) Non-enzymatic glucose sensor composed of carbon-coated nano-zinc oxide. *Nanomaterials* **7**, 36.
26. Daniel M, Mathew G, Anpo M, Neppolian B (2022) MOF based electrochemical sensors for the detection of physiologically relevant biomolecules: An overview. *Coordin Chem Rev* **468**, 214627.
27. Qian Q, Asinger PA, Lee MJ, Han G, Rodriguez KM, Lin S, Benedetti FM, Wu AX, et al (2020) MOF-based membranes for gas separations. *Chem Rev* **120**, 8161–8266.
28. Li WH, Lv J, Li Q, Xie J, Ogiwara N, Huang Y, Jiang H, Kitagawa H, et al (2019) Conductive metal-organic framework nanowire arrays for electrocatalytic oxygen evolution. *J Mater Chem A* **7**, 10431–10438.
29. Cao LA, Yao MS, Jiang HJ, Kitagawa S, Ye XL, Li WH, Xu G (2020) A highly oriented conductive MOF thin film-based Schottky diode for self-powered light and gas detection. *J Mater Chem A* **8**, 9085–9090.
30. Yao MS, Li WH, Xu G (2021) Metal-organic frameworks and their derivatives for electrically-transduced gas sensors. *Coordin Chem Rev* **426**, 213479.
31. Yao MS, Cao LA, Tang YX, Wang GE, Liu RH, Kumar PN, Wu GD, Deng WH, et al (2019) Gas transport regulation in a MO/MOF interface for enhanced selective gas detection. *J Mater Chem A* **7**, 18397–18403.
32. Yao MS, Tang WX, Wang GE, Nath B, Xu G (2016) MOF thin film-coated metal oxide nanowire array: Significantly improved chemiresistor sensor performance. *Adv Mater* **28**, 5229–5234.
33. Mei H, Xie J, Li Z, Lou C, Lei G, Liu X, Zhang J (2022) Rational design of ZnO@ZIF-8 nanoarrays for improved electrochemical detection of H₂O₂. *CrystEngComm* **24**, 1645–1654.
34. Muthusankar E, Wabaidur SM, Alotman ZA, Johan MR, Ponnusamy VK, Ragupathy D (2020) Fabrication of amperometric sensor for glucose detection based on phosphotungstic acid-assisted PDDPA/ZnO nanohybrid composite. *Ionics* **26**, 6341–6349.
35. Lawrence Mary K, Vijila Manonmani J, Shobanadevi N, Janaki Ramya A (2023) Construction of a novel ZnO/rGO hybrid composite for efficient degradation of Cr(VI) and Cr(III) under visible light irradiation. *J Indian Chem Soc* **100**, 100890.
36. Niu X, Lan M, Zhao H, Chen C (2013) Highly sensitive and selective nonenzymatic detection of glucose using three-dimensional porous nickel nanostructures. *Anal Chem* **85**, 3561–3569.
37. Qiao Y, Liu Q, Lu S, Chen G, Gao S, Lu W, Sun X (2020) High-performance non-enzymatic glucose detection: using a conductive Ni-MOF as an electrocatalyst. *J Mater Chem B* **8**, 5411–5415.
38. Hou Q, Wu Y, Zhou S, Wei Y, Caro J, Wang H (2019) Ultra-tuning of the aperture size in stiffened ZIF-8 MOF frameworks with mixed-linker strategy for enhanced CO₂/CH₄ separation. *Angew Chem Int Ed Engl* **58**, 327–331.
39. Kolokolov DI, Stepanov AG, Jobic H (2015) Mobility of the 2-methylimidazole linkers in ZIF-8 probed by ²H NMR: Saloon doors for the guests. *J Phys Chem C* **119**, 27512–27520.
40. Cai B, Zhou Y, Zhao M, Cai H, Ye Z, Wang L, Huang J (2014) Synthesis of ZnO-CuO porous core-shell spheres and their application for non-enzymatic glucose sensor. *Appl Phys A* **118**, 989–996.

Appendix A. Supplementary data

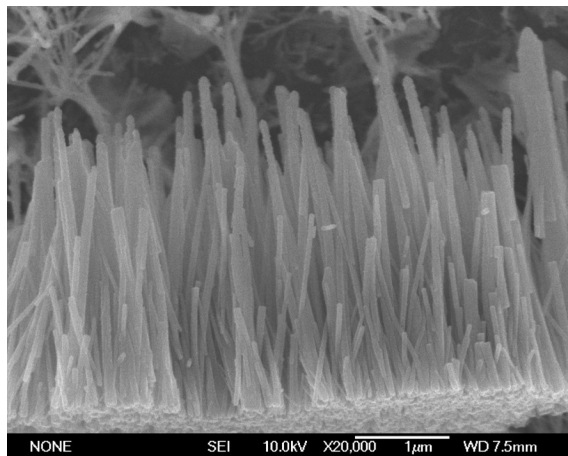


Fig. S1 Cross section view SEM image of ZnO@ZIF-67 nanowire array.

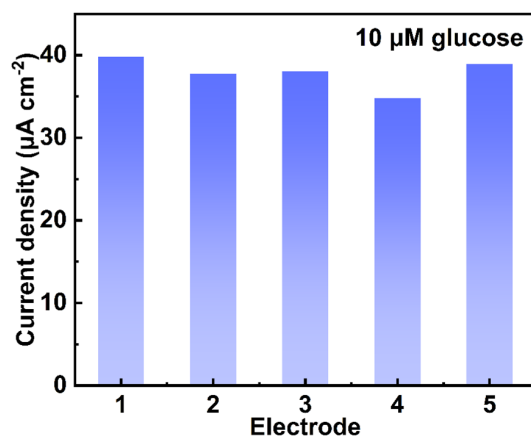


Fig. S2 Response current density of five different ZnO@ZIF-67/ITO electrodes toward 10 µM glucose.

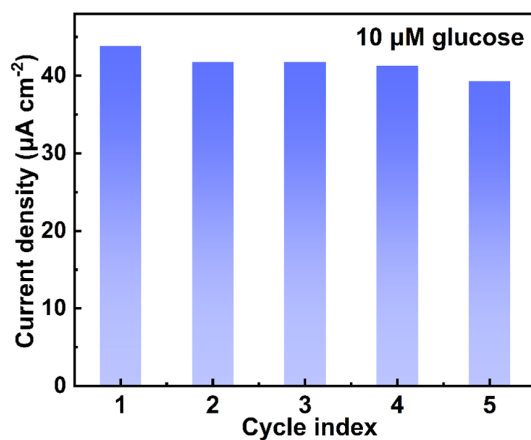


Fig. S3 Response current density of ZnO@ZIF-67/ITO electrode toward 10 µM glucose for five continuous tests.

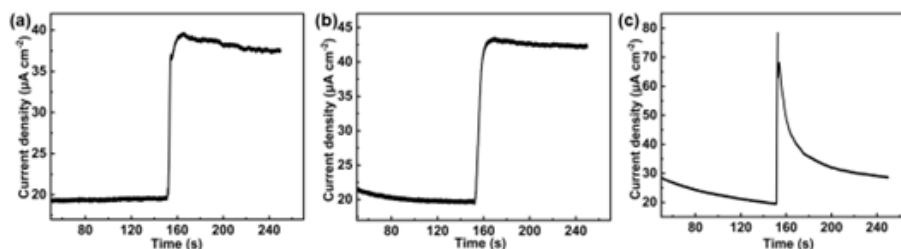


Fig. S4 (a–c) The amperometric curves for glucose in human serum which was obtained by the ZnO@ZIF-67/ITO electrode and repeated for 3 times.

Table S1 Determination of glucose concentration in human serum samples by ZnO@ZIF-67/ITO electrode.

Measured by medical equipment (mM)	Test result (mM)	RSD (%)	Recovery (%)
6.20	6.30	3.33	101.60
	6.54		105.48
	6.12		98.71

Table S2 Comparison of the performance of recently developed ZnO-based sensor platforms for non-enzymatic glucose detection.

Sensor	Electrochemical method	Sensitivity ($\mu\text{A cm}^{-2}\text{Mm}^{-1}$)	Linear range (mM)	Detection limit (μM)	Ref.
Au-ZnO/GOx	Amperometry	24.613	0.1–7.1	5	1
ITO-ZnO/GOx	Amperometry	–	0.005–0.3	3	2
GCE-ZnO/GOx	Amperometry	65.82	0.005–13.15	1	3
ITO-ZnO/GOx/Pt/CHIT	CV	62.14	0.1–2	16.6	4
GCE-ZnO/Ag/Graphen	CV	–	0.1–12	10.6	5
ZnO nanocombs	Amperometry	1533	0.02–4.5	20	6
ZnO-Ag	Amperometry	3.85	0.015–6.5	1.5	7
ZnO-Co	Amperometry	13.3	0–4	20	8
ZnO/carbon	Amperometry	2.97	0.1–10	1000	9
Ag@ZIF-67/GCE	CV	379	0.002–1	0.66	10
Ag@TiO ₂ @ZIF-67	CV	788	–	0.99	11
ITO-ZnO@ZIF-67	Amperometry	532.24	0.005–0.55	1.6	This work

REFERENCES

- Umar A, Rahman MM, Kim SH, Hahn YB (2008) ZnO nanonails: Synthesis and their application as glucose biosensor. *J Nanosci Nanotechnol* **8**, 3216–3221.
- Liu X, Hu Q, Wu Q, Zhang W, Fang Z, Xie Q (2009) Aligned ZnO nanorods: a useful film to fabricate amperometric glucose biosensor. *Colloids Surf B Biointerfaces* **74**, 154–158.
- Fang B, Zhang C, Wang G, Wang M, Ji Y (2011) A glucose oxidase immobilization platform for glucose biosensor using ZnO hollow nanospheres. *Sens Actuators B Chem* **155**, 304–310.
- Anusha JR, Kim HJ, Fleming AT, Das SJ, Yu KH, Kim BC, Raj CJ (2014) Simple fabrication of ZnO/Pt/chitosan electrode for enzymatic glucose biosensor. *Sens Actuators B Chem* **202**, 827–833.
- Li Z, Sheng L, Meng A, Xie C, Zhao K (2016) A glassy carbon electrode modified with a composite consisting of reduced graphene oxide, zinc oxide and silver nanoparticles in a chitosan matrix for studying the direct electron transfer of glucose oxidase and for enzymatic sensing of glucose. *Mikrochim Acta* **183**, 1625–1632.
- Wang JX, Sun XW, Wei A, Lei Y, Cai XP, Li CM, Dong ZL (2006) Zinc oxide nanocomb biosensor for glucose detection. *Appl Phys Lett* **88**, 233106.
- Zhou F, Jing W, Liu P, Han D, Jiang Z, Wei Z (2017) Doping Ag in ZnO nanorods to improve the performance of related enzymatic glucose sensors. *Sensors (Basel)* **17**, 102214.
- Zhao ZW, Chen XJ, Tay BK, Chen JS, Han ZJ, Khor KA (2007) A novel amperometric biosensor based on ZnO: Co nanoclusters for biosensing glucose. *Biosens Bioelectron* **23**, 135–139.
- Chung RJ, Wang AN, Liao QL, Chuang KY (2017) Non-enzymatic glucose sensor composed of carbon-coated nano-zinc oxide. *Nanomaterials* **7**, 7020036.
- Meng W, Wen YY, Dai L, He ZX, Wang L (2018) A novel electrochemical sensor for glucose detection based on Ag@ZIF-67 nanocomposite. *Sens Actuators B Chem* **260**, 852–860.
- Arif D, Hussain Z, Sohail M, Liaquat MA, Khan MA, Noor T (2020) A Non-enzymatic electrochemical sensor for glucose detection based on Ag@TiO₂@ metal-organic framework (ZIF-67) nanocomposite. *Front Chem* **8**, 573510.